Atmospheric trends of long-lived halogenated gases derived from 15 years of IASI measurements

Hélène de Longueville, Lieven Clarisse, Simon Whitburn, Cathy Clerbaux, Gilles Lecomte, Pierre-François Coheur

Journal of Quantitative Spectroscopy & Radiative Transfer 311 (2023) 108755

Contents lists available at ScienceDirect

Journal of Quantitative Spectroscopy and Radiative Transfer

journal homepage: www.elsevier.com/locate/jqsrt

Atmospheric trends of long-lived halogenated gases derived from 15 years of IASI measurements

Hélène De Longueville [a,*], Lieven Clarisse [a], Simon Whitburn [a], Cathy Clerbaux [a,b], Gilles Lecomte [a], Pierre Coheur [a]

[a] Université libre de Bruxelles (ULB), Spectroscopy, Quantum Chemistry and Atmospheric Remote Sensing (SQUARES), Brussels, Belgium
[b] LATMOS/IPSL, Sorbonne Université, UVSQ, CNRS, Paris, France

ARTICLE INFO

Keywords:
Long-lived halogenated gases
IASI/Metop
Generalized least squares estimation
Atmospheric concentration

ABSTRACT

Atmospheric emissions of chlorofluorocarbons (CFCs), their hydrogenated derivatives (HCFCs, HFCs) and other long-lived halogen-containing substances perturb the chemical and radiative equilibrium of our atmosphere. A global network of ground-based stations (AGAGE) monitors the concentrations of most of these species. Supplementing these, upper tropospheric and stratospheric concentrations are available from satellite measurements of the ACE-FTS solar occultation sounder. Measurements derived from nadir viewing infrared sounders can potentially complement both observational datasets, offering extensive spatial coverage and temporal sampling. With a preferential sensitivity to the middle troposphere, they also cover the vertical altitude range that is not covered by other means. However, fluctuations in surface temperature and the concentration of interfering atmospheric constituents render the retrieval of halogenated species particularly challenging. Relying on previous work on spectral whitening, we present an unconstrained generalized least squares estimation retrieval methodology, which largely allows to overcome the problem of interference. We demonstrate that it can be used to retrieve monthly anomalies of all halogenated species previously observed in spectra from the Infrared Atmospheric Sounding Interferometer (IASI/Metop). Focussing on northern mid-latitudes, we derive the monthly concentrations of CFC-11, CFC-12, HCFC-22, HCFC-142b, HFC-134a, CF_4, SF_6 and CCl_4 between 2008 and 2022. Trends are compared to the observations from AGAGE and ACE-FTS. A good match is obtained with both, with especially remarkable agreement in the linear trends for CF_4, SF_6 and HFC-134a, and in the non-linear trends of CFC-11 and HCFC-22. Large discrepancies and unexplained variations are seen in the time series of HCFC-142b, CFC-12 and CCl_4, necessitating further optimization of the retrieval technique. The results demonstrate the potential of IASI and follow-up missions for establishing a unique long-term time series of the most important long-lived halogenated species.

1. Introduction

Long-lived halogenated gases are potent greenhouse gases and contribute, for chlorinated and brominated compounds, to the depletion of stratospheric ozone and to the development of the Antarctic ozone hole [1]. The production of many of these halogen-containing species is therefore, since years, controlled by the Montreal Protocol on Substances that Deplete the Ozone Layer and its amendments [2]. This is in particular the case for the long-lived chlorofluorocarbons (CFCs) and CCl_4, powerful ozone depleting substances which were widely used as refrigerants, aerosol propellants, solvents and blowing agents until the beginning of the 21st century. Their production has been banned worldwide in 2010. The first and transitional substitutes to the CFCs were the hydrochlorofluorocarbons (HCFCs), which have a lower potential for ozone depletion because of their much larger degradation rate in the troposphere. HCFCs are being phased out and their production is completely banned in developed countries since 2020 [3]. CFCs and HCFCs are currently being replaced in several applications by chlorine-free hydrofluorocarbons (HFCs). Although harmless for stratospheric ozone, HFCs contribute to global warming and, to ensure that they do not counteract the climate benefits achieved by reducing the emissions of CFCs and HCFCs, they have been included in 2016 in the list of controlled substances under the Kigali amendment to the Montreal Protocol. It is worth pointing out that in view of their importance in the Earth's climate, additional controls have been set within the Kyoto protocol, superseded by the Paris Agreement, on HFCs, and other chlorine-free compounds: perfluorocarbons (PFCs) and SF_6 [3,4].

* Corresponding author.
E-mail address: Helene.De.Longueville@ulb.be (H. De Longueville).

https://doi.org/10.1016/j.jqsrt.2023.108755
Received 8 May 2023; Received in revised form 17 August 2023; Accepted 17 August 2023
Available online 23 August 2023

A continuous observing network is essential to monitor the atmospheric abundances of long-lived halogenated gases (ideally in different latitude bands but also at different altitudes), to evaluate the effectiveness of international regulations with regard to emissions, and ultimately to assess the environmental impacts of the changes at play. The Advanced Global Atmospheric Gases Experiment (AGAGE) has been measuring the composition of the global atmosphere continuously since 1978. It currently provides the longest and most accurate time series of halogenated gases abundances, next to the US NOAA (National Oceanic and Atmospheric Administration) network which also serves a similar function [5]. The AGAGE data have been and are still central for quantifying long-term trends in halogen-containing compounds [5] and the response of the atmosphere to changes in emissions. Examples include the recent CFC-11 saga [6,7], or the global increase of minor CFCs over the past decade [8]. Even though AGAGE and NOAA are invaluable networks, they are limited in coverage by the number of ground-based stations. These are particularly scarce in low- and middle-income regions, where emissions are likely to rise as countries develop [9]. Provided it is sufficiently accurate, a global monitoring system based on dense space observations would therefore favorably complement the ground-based network and help tracking emissions (possibly unreported) locally and regionally.

Recently, high-resolution IR remote sensing measurements from the ground or satellites, were shown to favorably supplement the in situ measurement network. Time evolutions in the abundance of several halogenated species have been acquired from ground-based Fourier Transform Infrared measurements, with, for some, an accuracy sufficient to precisely identify break points and relate these to changes in emissions (e.g., [10–13]). Similarly, IR measurements from satellites offer the possibility to quantify the concentrations of several halogenated gases (e.g., [14–17]). The high-resolution Fourier Transform Spectrometer from the Atmospheric Chemistry Experiment (ACE-FTS), which operates in solar-occultation mode, has in particular been pioneering, with the monitoring of up to 16 ozone depleting substances and other halogenated species over a 15-year period [18]. Reliable latitude–altitude distributions were obtained for most compounds [18] and emissions were successfully inverted from the yearly measurements for eight substances controlled by the Montreal protocol [19]. The ACE-FTS is still in operation today and will soon have a 20-year worth of measurement available in the upper troposphere and the stratosphere. Although the measurements from hyperspectral IR nadir sounders also contain information on several long-lived halogenated gases [14,20,21], they have not been extensively exploited so far for quantitative retrieval and even more so for trend analyses. Nadir observations have a lower signal-to-noise than solar-occultation measurements, but have the advantage of being sensitive to the middle troposphere and also have a much denser spatial coverage, at all latitudes. They offer therefore the possibility of reducing the retrieval uncertainties associated with individual measurements by spatial and or temporal averaging. Finally, they also have the potential to improve monitoring with a spatial coverage at the surface superior than any existing ground-based networks. Recently, Chen et al. [22] applied to the measurements from the Atmospheric IR Sounder (AIRS) a simple double differential method along with a look-up-table approach to retrieve surface concentrations of CFC-11. They have exploited a 15-year record of AIRS measurements to map trends in 30° longitude by 10° latitude grid boxes between 55°S and 55°N. A slowdown in the CFC-11 rate of decrease was reported, consistently with the other observation means.

In this work, we use a similar 15-year record (2008–2022) of measurements from the Infrared Atmospheric Sounding Interferometer (IASI) on board the Metop series of platforms to determine trends in the concentrations of several long-lived halogenated species. For this we rely on a very sensitive detection methodology described by De Longueville et al. [20] and on a quantification method described in Section 2. The trends are obtained for eight species, i.e., CFC-11 ($CFCl_3$), CFC-12 (CF_2Cl_2), HCFC-22 (CHF_2Cl), HCFC-142b (CH_3CF_2Cl), HFC-134a (CH_2FCF_3), carbon tetrafluoride (CF_4), sulfur hexafluoride (SF_6) and carbon tetrachloride (CCl_4). They are discussed and evaluated in Section 3.

2. Methods

2.1. Revealing changes through spectral whitening

Flying on-board the Metop-A/B/C platforms, the IASI instruments provide continuous measurements since 2007 [23], with remarkable stability for the nadir radiance (Level 1C) observations. The latter are calibrated and span the spectral range from 645 to 2760 cm^{-1} without gaps, sampled at 0.25 cm^{-1}. Owing to a wide swath, IASI offers quasi-global coverage bi-daily with high horizontal resolution (~12 km at nadir). While IASI-A has ceased operations in 2021, IASI-B and IASI-C are still operating nominally and should extend the climate record of radiances at least until 2025, when the new generation of hyperspectral instruments (IASI-NG) will take over [24]. This continuity in the measurements makes IASI particularly useful for trend assessment [25–30].

Long-lived halogenated species have a weak spectral signature in the Earth's outgoing longwave radiation, which makes their detection in individual spectra challenging [31]. In [20], it was shown that a particular type of spectral transformation, called whitening, allows for the identification of eight halogen-containing species in IASI mean spectra (listed in previous section). Three of these (i.e., HCFC-142b, HFC-134a, SF_6) were never detected before. Much better than other techniques, whitening is well suited to efficiently remove the largest and most variable spectral features due to e.g., O_3, CO_2, N_2O, CH_4 and H_2O that are seen in each spectrum, allowing for the detection of weak and slowly varying features.

Whitening relies crucially on a dataset of reference spectra, characterized by a mean spectrum $\bar{y}$ and a covariance matrix S. With these, the whitening transform of a spectrum y is defined as

$$\tilde{y} = S^{-\frac{1}{2}}(y - \bar{y}). \tag{1}$$

By construction $\tilde{y}$ has a mean of zero and a standard deviation of one on spectra originating from the reference dataset. Whitening can be seen as a type of normalization, removing the mean from each spectrum and inversely weighting each channel with its expected variability. At the same time it serves to decorrelate the different spectral channels [32]. What remains is a spectral residual of anomalies with respect to the given reference dataset. De Longueville et al. [20] showed that spectral changes in long-lived halogenated species can be revealed by applying whitening on mean spectra from a different time period than the one from the reference dataset from which the pair $\{S, \bar{y}\}$ is computed.

We illustrate this in Fig. 1, where whitening is applied on five mean spectra calculated from clear-sky IASI-A spectra measured in June 2008, 2011, 2015, 2018 and 2021 over ocean at northern mid-latitudes. The mean spectrum from June 2008 was chosen as reference spectrum $\bar{y}$ while the covariance matrix was built using a subset of spectra measured throughout 2008 over the same region. Large residuals are seen to gradually appear from 2008 to 2021, with positive (negative) values indicating a progressive decrease (increase) in atmospheric absorption. Specific spectral features can be matched to atmospheric species, by comparison with a Jacobian, i.e., the derivative of the climatological background spectrum with respect to changes in concentration. In the case of whitened spectra, the comparison should be made with whitened Jacobians $\tilde{K} = S^{-\frac{1}{2}}K$ [20].

In this way, CFC-11, CFC-12 and CCl_4 are readily identified in the figure with increasing residuals, which correspond to a decrease in atmospheric concentrations between 2008 and 2021. This is corroborated by a host of other observations [2] and follows the global effort to reduce their emissions. Five other halogenated species are detected (HCFC-22, HCFC-142b, HFC-134a, CF_4 and SF_6), all with negative residuals, consistent with their current atmospheric increase. Finally, several absorption lines of CO_2 are seen, also with a negative value, and again consistent with its positive trend.

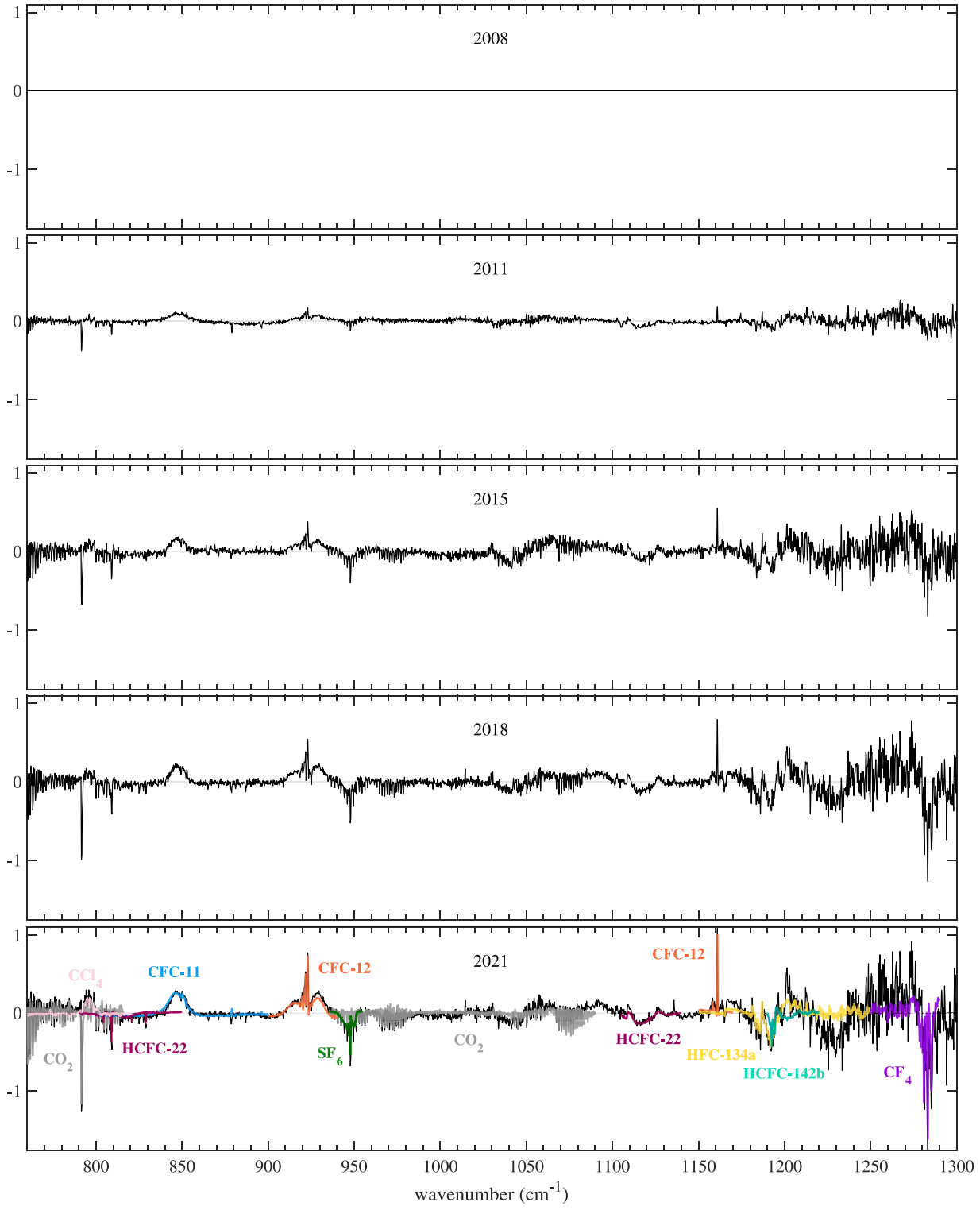

Fig. 1. Whitened spectra over ocean at northern mid-latitudes from June 2008, 2011, 2015, 2018, 2021 revealing eight long-lived halogenated species and carbon dioxide in the 760–1300 cm^{-1} spectral range. The year 2008 is used as a reference. For each detected species, its Jacobian is reported over the spectral range selected for its retrieval (see Table 1).

2.2. Generalized least squares estimation

Whitening allows effective detection and verification of specific spectral signatures, however for a quantitative retrieval, another technique is required. Here, we apply the (unconstrained) generalized least squares method [33,34]. This method is similar to conventional unconstrained least squares estimation [35],

$$\hat{x} = x_0 + (K^T S^{-1} K)^{-1} K^T S^{-1} (y - \bar{y}) \quad (2)$$

(with $\hat{x}$ and x_0 the retrieved and reference concentrations of the target species), except that the usual noise covariance matrix S_e is replaced by a generalized noise covariance matrix S. When this matrix characterizes all expected spectral variability around $\bar{y}$, except the one related to the target species, it can be shown that the retrieval is theoretically equivalent to a regular unconstrained least squares retrieval, where in addition to the target species, all unknown parameters affecting the spectrum are retrieved simultaneously [33–36]. In practice however, not having to retrieve other parameters has significant advantages. Firstly, the regular least squares is only valid in the linear regime and as such rarely applied. For that reason, the retrieval formula has to be adapted so that a solution is achieved iteratively (e.g., Gauss–Newton method), with the associated computational cost. The generalized least squares method, on the other hand, can far more often be applied as a one-step retrieval, as long as the spectrum behaves linearly with respect to changes in the target species. A second major advantage is that the impact of forward modeling errors (related to both surface and atmosphere) are reduced, as their variations are effectively modeled by the use of the generalized noise covariance matrix. This is particularly the case when S and $\bar{y}$ are derived from real spectra.

The generalized least squares estimation method has been successfully applied for the retrieval of SO_2, both in the infrared [34] and the UV/Vis [37]. For this use case, a generalized covariance matrix and associated mean spectrum $\bar{y}$ can be constructed from observed spectra without detectable SO_2. For the well-mixed and long-lived species of interest here, this is not possible, as their signatures are present in all clear-sky spectra. However, inspired by the successful application of the whitening transformation, we can build the covariance and associated mean from spectra originating from a given time period, allowing the retrieval of their concentrations in other time periods. An important boundary condition is that the concentration corresponding to the reference period, x_0, needs to be known. Here, we rely on ground-based measurements from the AGAGE network to calibrate the retrieved concentrations.

2.3. Retrieval setup

The generalized least squares estimation is a powerful one-step retrieval. However, its success depends critically on a careful setup of the reference dataset for the calculation of the $\bar{y}$ and S, the selection of the retrieval parameters (e.g., spectral range) and the calculation of Jacobians.

For the calculation of the Jacobians K, a scene specified by surface and atmospheric parameters is required, that should be as close as possible to the true state of the atmosphere. Temperature is particularly important, as it drives the sensitivity, and thus the signal strength. A separate Jacobian is therefore ideally calculated for each observation. However, to reduce the computational burden, and to increase the signal to noise ratio, the retrieval can be performed on averaged spectra using average Jacobians. It is important in that case, to keep the variability in the dataset that is averaged as small as possible, so that the average Jacobian is representative for average scene conditions. For this reason, it was decided to work with monthly averages and to focus on observations over ocean at northern mid-latitudes (23.27°N–66.32°N). To further increase homogeneity, only clear-sky observations with a viewing angle below 15° were considered. Clouds were flagged with a recently developed cloud product, that was specifically developed for trend and climate studies [38].

Monthly reference spectra $\bar{y}$ were obtained by averaging observations from 2008 from six days per month (the 1st, 5th, 10th, 15th, 20th and 25th of each month), corresponding to about 35,500 spectra per month. All other monthly spectra y from which the concentrations are retrieved, were obtained in the same way, but then for the years between 2009 and 2022, and for each of the three IASI instruments, when available. Before 2017, IASI-A L1c reprocessed data were used [39]. A single generalized covariance matrix was constructed from all 430,000 reference spectra of 2008.

The retrieval was ran separately for each of the eight identified long-lived halogenated species, using specific spectral ranges. The latter were selected on the basis of the whitened spectra shown in Fig. 1, making sure that it also included a region largely unaffected by the absorption of halogenated species, to serve as a reference for the baseline. Overall, a compromise was sought between maximizing the range and minimizing interference with other long-lived species. Indeed, while the use of the generalized covariance matrix eliminates the need to retrieve surface temperature and species exhibiting large variability, by construction, all interfering species displaying a trend in the time period investigated (halogenated species, CO_2 and HNO_3) need to be co-retrieved as their variations are not accounted for in the covariance matrix. For the simultaneous retrieval of several species, Eq. (2) remains formally identical, but K becomes a matrix with multiple columns, and $\hat{x}$ and x_0 become vectors of retrieved and reference concentrations. The chosen spectral windows and the associated interfering species are given in Table 1.

For the calculation of the Jacobians, forward simulations were performed with the Atmosphit radiative transfer code [40] relying on the HITRAN database 2012 for all spectroscopic parameters (cross sections, line parameters) [41]. For the calculation of monthly representative Jacobians, full scene conditions are required and this input data was gathered as follows. Monthly averaged surface temperature, pressure, temperature and humidity profiles over the zone of interest were calculated from the ERA5 reanalysis output [42–44] for the year 2008. For other important tracers, such as O_3 and CH_4 averaged profiles from [45] were used. For the halogenated species of interest, averaged global profiles were calculated from 2008–2022 ACE-FTS v5.0 Level 2 data [16,46]. Given the larger retrieval uncertainty of ACE-FTS at lower altitudes, and as no sharp gradients are expected in the troposphere for the species of interest, data below 8.5 km was replaced by the value at 8.5 km. In the case of HCFC-142b, the cut-off altitude was set to 14.5 km to avoid a local maximum at this altitude which does not match other observations. These profiles are given in Fig. 2. Finally, the profiles were shifted to match the monthly surface concentration of AGAGE in 2008, obtained by averaging the in situ measurements from sites located at northern mid-latitudes: Mace Head (Ireland), Jungfraujoch (Switzerland), Monte Cimone (Italy), Trinidad Head (California), Gosan (South Korea) [5]. An average zenith angle of 7.5° was used for the calculation of the Jacobian. Note that while IASI is sensitive to the total concentration over the column, rather than surface concentrations, the Jacobians were expressed in units of radiance per surface concentration, so that the retrieval immediately provides estimates of the surface concentration.

2.4. Time series and intercomparison

To retrieve monthly atmospheric concentrations, the generalized least squares estimation is applied on IASI monthly averaged spectra. The IASI-B and IASI-C concentrations were shifted to match IASI-A concentrations in their first operational year. Retrieved concentrations were averaged over the three sounders to get one value per month. Annual trends were derived from the retrieved time series using ordinary least squares, for the period 2008–2021. The estimated error on the

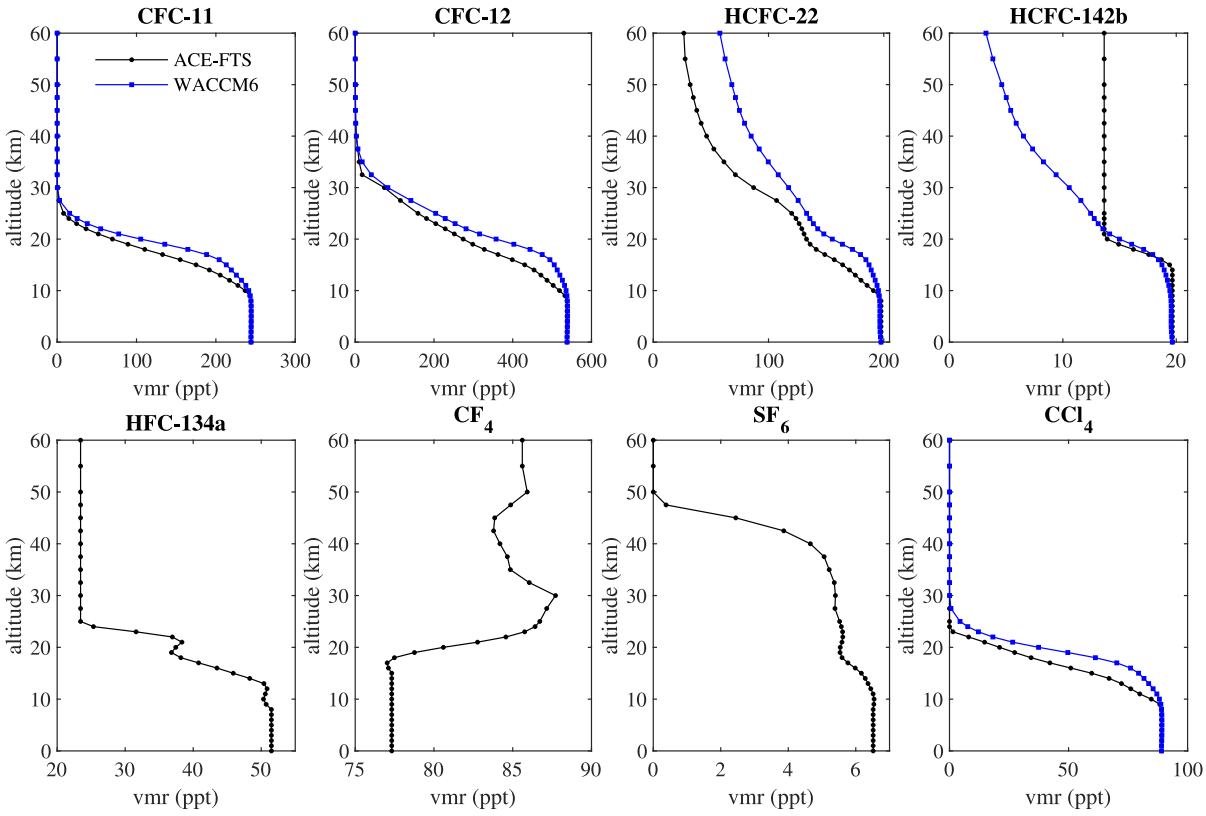

Fig. 2. Vertical profiles measured by ACE-FTS and modeled by WACCM6 of CFC-11, CFC-12, HCFC-22, HCFC-142b, HFC-134a, CF_4, SF_6 and CCl_4. The ACE-FTS profiles are global averages for the period 2008–2022, and the WACCM6 profiles are averages of two profiles modeled for two different locations in northern mid-latitudes (Toronto 44°–79°W in Canada and Tsukuba 36°–140°E in Japan).

Table 1
Retrieval parameters.

Target	Spectral range (cm^{-1})	Interfering species
CFC-11	800–900	CO_2, HNO_3, HCFC-22, CCl_4
CFC-12	900–940	CO_2, HNO_3, CFC-11, HCFC-142b, SF_6
HCFC-22	790–850	CO_2, CFC-11, CCl_4
HCFC-142b	1190–1220	HFC-134a
HFC-134a	1150–1250	CFC-12, HCFC-142b
CF_4	1250–1290	HCFC-142b, HFC-134a
SF_6	935–955	CO_2, CFC-12
CCl_4	760–820	CO_2, HNO_3, HCFC-22

trend was calculated as the root-mean-square error (RMSE) divided by the half-period (see Appendix for further information).

In the result section, we intercompare the retrieved concentrations and trends with observations from the in situ measurements network AGAGE and the solar occultation sounder ACE-FTS. For AGAGE, the monthly surface concentrations averaged over sites located at northern mid-latitudes were used to calculate reference trends. For the year 2008, these are the same ones as used for the reference concentration x_0 in Eq. (2). For ACE-FTS, averaged quarters concentrations (March–May, June–August, September–November, December–February) were built from v5.0 Level 2 data using the methodology from [16], where for each species all ACE-FTS retrievals are averaged over specific altitude range and latitudes, as specified in Table 2. An exception is CFC-12 for which the v5.0 shows high biases below 10 km. We therefore use the previous version (v4.1.2) for this species.

Table 2
ACE-FTS retrieval altitude ranges and latitudes from [16].

Target	Latitude range	Altitude range (km)
CFC-11	60°S–60°N	5.5–10.5
CFC-12	60°S–60°N	5.5–10.5
HCFC-22	60°S–60°N	5.5–10.5
HCFC-142b	60°S–60°N	6.5–10.5
HFC-134a	30°S–30°N	11.5–17.5
CF_4	60°S–60°N	25.5–40.5
SF_6	30°S–30°N	12.5–17.5
CCl_4	30°S–30°N	8.5–10.5

3. Results and discussion

The temporal evolutions in the abundances of the eight halogenated species identified in the whitened IASI spectra (Fig. 1) are shown in Fig. 3 for CFC-11, CFC-12, HCFC-22 and HCFC-142b; and in Fig. 4 for HFC-134a, CF_4, SF_6 and CCl_4. The abundances, which are expressed in volume mixing ratios (vmrs) following Eq. (2), are also compared in both Figures to those measured in situ at the AGAGE stations and from space by ACE-FTS. Because of the reference chosen to calculate the vmrs, our retrieved values match those of AGAGE for the first year of the measurements. The differences in the vmrs with ACE-FTS, which is seen for most species as a bias throughout the time period (exceptions are CFC-12 and CCl_4 for which the difference is time-dependent), are likely attributable to the specific altitudes probed by the instruments, i.e., a total column in the case of IASI and an average mixing ratio for the upper troposphere — lower stratosphere in the case of ACE-FTS (Table 2), combined with the species tropospheric lifetime. In that respect, it is interesting to see that differences are largest, at around 10 ppt for the first reference year, for the three hydrogenated compounds, which experience tropospheric oxidation.

An additional reason for the shift seen in the ACE-FTS data is that the associated dataset includes observations from both north and south hemispheres (Table 2) while the IASI and AGAGE datasets are built from northern mid-latitudes measurements exclusively, introducing a difference for species exhibiting an interhemispheric difference. Another point worth mentioning is the much larger variability of the IASI vmrs compared to those of AGAGE and ACE-FTS, which is related to the weak signal-to-noise of the measurements, and the presence of more spectral interferences. In addition, for some species (CF_4 and HCFC-22 in particular) recurrent intra-annual patterns remain, despite the fact that monthly Jacobians are used. As we discuss below for the different families of compounds, these do not prevent the calculation of trends with reasonable accuracy. Unless otherwise indicated, the trend values are obtained similarly for the three datasets by linear regression through all data points for the 2008–2021 period; they are given inset of Figs. 3 and 4 (the linear regression lines are also shown) and summarized in Table 3. Also listed in Table 3 is the normalized root-mean-square error (NRMSE) which characterizes the deviation of the retrieved vmrs from the linear regression model, normalized by the average vmr to facilitate the comparison between species. A NRMSE of zero indicates a perfect linear fit of the data while large NRMSE values reflect the poor ability of the model to accurately reproduce the data. Among the eight species of interest, CF_4 has the lowest NRMSE (0.005) and HCFC-142b has the highest NRMSE (0.06). This indicates that the trends for CF_4 and HCFC-142b are determined with the highest and lowest accuracy, respectively.

CFCs. CFC-11 and CFC-12 are the two most abundant CFCs in the atmosphere. In response to the Montreal Protocol, their atmospheric abundance is decreasing since 2000, and that decrease is well seen in Fig. 3 for the time period considered here, with vmrs at 219 ppt and 487 ppt in 2021 compared to 245 ppt and 539 ppt in 2008, respectively. Using a linear regression through the monthly vmrs derived from IASI, we find for CFC-11 a rate of decrease amounting −1.6 ppt/year during 2008–2021, with an uncertainty of ± 0.4 ppt/year. This trend value is in excellent agreement with the one from AGAGE which is −1.6 ± 0.1 ppt/year for the same period. It is also matching within the uncertainty the −1.5 ± 0.2 ppt/year trend from ACE-FTS. As explained in the introduction, the case of CFC-11 is of particular interest in view of the reported slowdown of the decrease between 2012 and 2019, possibly due to illegal emissions [1,6,7,47,48]. To see if these two breakpoints in the time evolution could be seen with IASI we have compared the trends for three separate periods: 2008–2011, 2012–2018 and 2019–2022 and found values of respectively −3 ± 1 ppt/year, −1.3 ± 0.6 ppt/year and −4 ± 1 ppt/year. Despite the fact that the trends for the first and third periods (that only span four years) come with larger uncertainty, we observe clearly a slowdown in the decline after 2012 followed by a return to normal in 2019 with an even higher rate of decrease than before 2012. While this acceleration compared to pre-2012 will have to be confirmed in the future by extending the time series, the fact that the breakpoints are well identified demonstrates the ability of IASI to capture the changes in the rate of decrease.

For CFC-12, we calculate from the IASI time series a rate of −4.0 ± 0.8 ppt/year between 2008 and 2021, which is larger than that inferred from AGAGE (−3.2 ± 0.2 ppt/year) and even more from ACE-FTS (−2.8 ± 0.3 ppt/year). The reason for this discrepancy is not known at present but we suspect that it could be due to spectral interferences with another long-lived tracer absorbing in the atmospheric window between 900 and 940 cm^{-1}. Note also that on top of the already large monthly variability for CFC-12, we see a somewhat more pronounced outlier in October 2015 (note that the 2015 outlier is also seen for HCFC-142b). As a sanity check we have also tested the other spectral band of CFC-12 between 1150 and 1170 cm^{-1} (Fig. 1), to retrieve its vmrs and trend. The resulting trend is also larger than that of AGAGE and ACE-FTS. In fact it decreases even faster in this spectral region with a vmr of around 470 ppt in 2021. It is clear that more work will be needed to identify the cause of outliers in the CFC-12 time series from IASI and to improve its trend determination. To conclude for CFC-12, we find with IASI (with large uncertainty, Table 3), consistent with AGAGE and ACE-FTS, an acceleration of the rate of decrease with time with trends of −3 ± 2 ppt/year and −4 ± 1 ppt/year for the two sub-periods 2008–2011 and 2012–2021 considered.

HCFCs. As a consequence of the regulations put on the production of CFCs, transitional HCFCs, such as HCFC-22 and HCFC-142b, have been widely used, leading to an increase of their atmospheric abundance. Starting respectively from values of about 205 and 21 ppt in 2008 we find from IASI vmrs reaching maxima at the end of the time period, of around 262 ppt and 27 ppt after 2021. Having been regulated themselves by the Montreal Protocol, the rate of increase is progressively slowing down [1] and this shows up for HCFC-142b in particular, with a plateau after 2011. The linear regression applied over the entire 2008–2021 time period gives for HCFC-22 a growth rate of 4.5 ± 0.7 ppt/year, broadly consistent with AGAGE (4.2 ± 0.6 ppt/year) and ACE-FTS (4.5 ± 0.6 ppt/year). The rate of decrease has halved between 2008–2011 (7 ± 1 ppt/year) and 2012–2021 (3.5 ± 0.8 ppt/year). We have also tested the second spectral band of HCFC-22 between 1110 and 1130 cm^{-1}, which is also seen in the whitened IASI spectra (Fig. 1), to calculate a trend for the period 2008–2021, which gives a similar trend but with a larger variability (4 ± 1 ppt/year). This is likely due to weaker absorption in this spectral range, leading to a smaller signal-to-noise ratio.

HCFC-142b shows a much smaller positive trend of 0.3 ± 0.2 ppt/year between 2008–2021, which is furthermore not representative in view of the plateau appearing just after 2011 (the trend is close to zero after 2012; see Table 3). In that respect, the comparison with the trends obtained from the AGAGE (0.1 ± 0.1 ppt/year) and ACE-FTS (0.28 ± 0.09 ppt/year) datasets is also not relevant. Among the eight investigated species, HCFC-142b has the highest NRMSE (0.06) indicating it is the least well represented by linear regression. This is also true for AGAGE and ACE-FTS.

HFCs. The abundance of HFC-134a is increasing rapidly as a result of its intensive use in refrigeration and air conditioning systems, as a blowing agent for polyurethane foams, and as a propellant for medical aerosols. We find from IASI a vmr of 130 ppt in 2021, more than 2.4 times its 2008 value (54 ppt). The linear trend value for the 2008–2021 IASI period is 6.0 ± 0.3 ppt/year, surpassing that of HCFC-22. This trend is, taking into account the respective uncertainties, in good agreement with those from AGAGE (5.6 ± 0.2 ppt/year) and ACE-FTS (5.4 ± 0.3 ppt/year). It is worth noting that the error on the trend is smaller than for the above-discussed compounds, resulting from the much weaker variability in the retrieved monthly vmrs and the absence of a breakpoint in the time series, as seen from Fig. 4a.

PFCs and sulfur hexafluoride. CF_4, also named PFC-14, is one of the major PFCs and is emitted mostly from the industrial sector, following its use in aluminum and semiconductor production [49]. SF_6 is primarily used for electrical insulation and semiconductors [50]. Because of their extremely long lifetimes (850–1280 years for SF_6 and 50,000 years for CF_4 [1]), these compounds reach the mesosphere where they are photolyzed by UV radiation or, in the case of SF_6, degraded after electron attachment [51]. The abundance of these fluorinated species is also increasing steadily, although at a slower pace than HFC-134a. We find from IASI maximum vmrs around 88 ppt for CF_4 (Fig. 4b) and 11 ppt for SF_6 (Fig. 4c), resulting from a linear growth rate of 0.78 ± 0.06 ppt/year and 0.34 ± 0.03 ppt/year, respectively. As in the case of HFC-134a and for the same reasons, the error on the two trend values is particularly small and we find a remarkable agreement with the trends determined from AGAGE (0.80 ± 0.03 ppt/year for CF_4; 0.325 ± 0.007 ppt/year for SF_6) and ACE-FTS (0.75 ± 0.06 ppt/year for CF_4; 0.31 ± 0.02 ppt/year for SF_6). Among the species of interest, CF_4 has the lowest NRMSE (0.005) and is therefore the species which is best modeled by linear regression.

Carbon tetrachloride. CCl_4 has been regulated by the Montreal Protocol for as long as CFCs, leading to a decrease in its atmospheric

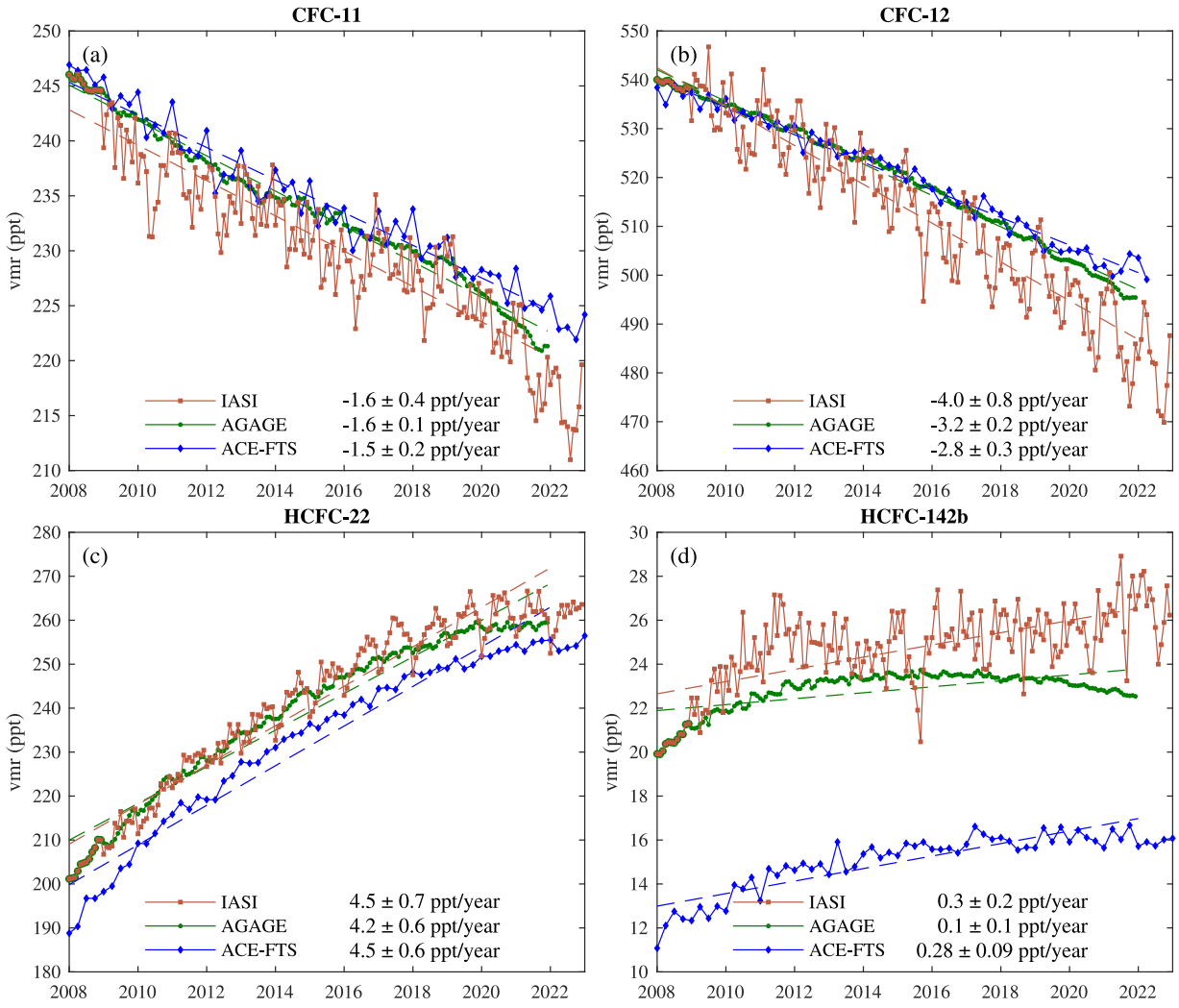

Fig. 3. IASI time series of CFC-11 (a), CFC-12 (b), HCFC-22 (c) and HCFC-142b (d) volume mixing ratio (ppt) in oceanic northern mid-latitudes over the period 2008–2022 and their declining (a, b) or growing (c, d) rate (ppt/year) between 2008–2021. AGAGE time series are averaged data from northern mid-latitudes AGAGE stations and ACE-FTS time series are global.

vmrs after a peak at around 105 ppt in the early 1990s [1]. Starting from a vmr value of around 89 ppt in 2008, we find a minimum vmr in 2021 of about 72 ppt, corresponding to a linear rate of decline of −1.3 ± 0.3 ppt/year over the 2008–2021 time period. While it comes with a small error, this negative trend is significantly larger than that inferred from the in situ measurements (−1.03 ± 0.04 ppt/year) and even more so from ACE-FTS (−1.0 ± 0.3 ppt/year). This might be due to the overlap with CO_2 in the region where CCl_4 is retrieved (see Fig. 1).

The methodology developed for inferring the trends from IASI, exposed in Section 2, heavily relies on the use of the spectral Jacobians for each species, which may be impacted by a series of factors, among which the assumption on the vertical concentration profiles. In order to assess how much a change in the vertical profile of the different species could impact the trend values, we have performed, for a new set of Jacobians, calculations relying this time on modeled profiles and used those to calculate the monthly vmrs as previously. The model profiles were obtained from the Whole Atmosphere Community Climate Model Version 6 [52,53] and correspond for each species to an average of two profiles modeled for two NDACC locations in northern mid-latitudes (Network for the Detection of Atmospheric Composition Change, De Mazière et al. [54]), namely Toronto (44°N–79°W, Canada) and Tsukuba (36°N–140°E, Japan). This model only provides data for CFC-11, CFC-12, HCFC-22, HCFC-142b and CCl_4 which are illustrated in Fig. 2. As can be seen in Table 4, the use of these modeled profiles instead of those from ACE-FTS produces differences in the trends of less than 8%, not affecting significantly the comparison with AGAGE.

4. Conclusion

Measurements from the series of IASI instruments, and follow-on missions, provide an opportunity to establish a unique long-term time series of important long-lived halogenated species. IASI's main assets are: (i) the high-quality of the radiance measurements and their exceptional stability and coherence over time, (ii) unmatched temporal sampling and spatial coverage of the measurements, (iii) the unique sensitivity of infrared nadir sounders to the middle troposphere, complementing in situ ground observations and upper tropospheric and stratospheric measurements from limb-sounders.

In a previous study, we exposed long-term changes in the spectral signature of long-lived halogenated species through spectral whitening [20]. This technique relies on a generalized covariance matrix to remove variations in surface temperature and concentration of large absorbers. Here, we employed the generalized least squares estimation retrieval technique, which relies on the same type of covariance

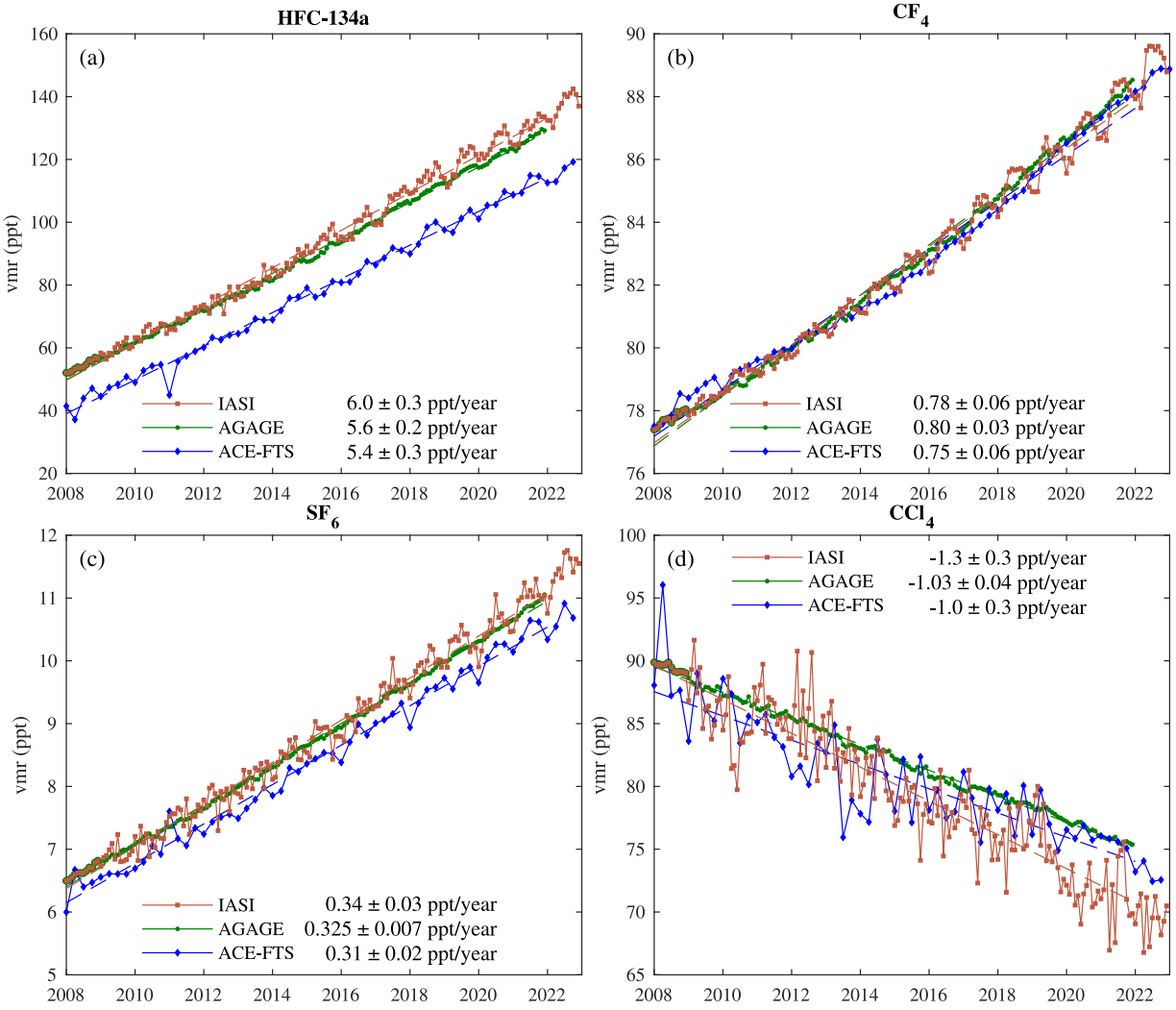

Fig. 4. IASI time series of HFC-134a (a), CF_4 (b), SF_6 (c) and CCl_4 (d) volume mixing ratio (ppt) in oceanic northern mid-latitudes over the period 2008–2022 and their growing (a, b, c) or declining (d) rate (ppt/year) between 2008–2021. AGAGE time series are averaged data from northern mid-latitudes AGAGE stations and ACE-FTS time series are global.

matrices, to quantitatively retrieve the atmospheric concentrations of halogenated gases. Compared to other techniques the main advantage is that it is a one-step approach, requiring no retrieval of other parameters affecting the measurement. Focusing on clear-sky IASI spectra observed over ocean at northern mid-latitudes for the period 2008–2022, atmospheric concentrations and trends were derived for eight long-lived halogenated species: CFC-11, CFC-12, HCFC-22, HCFC-142b, HFC-134a, CF_4, SF_6 and CCl_4 (six of which are controlled by the Montreal Protocol). The estimated linear trends show overall good consistency with those derived from the in situ measurements at AGAGE stations and the spatial observations of the ACE-FTS solar occultation sounder. However, too large discrepancies were found in the trends of CFC-12 and CCl_4, for reasons which are not entirely clear at the moment. It likely concerns variations in long-lived trace gases that are not taken into account by the retrieval method. Further, we demonstrated that IASI is able to capture the slowdown in the rate of decrease for CFC-11 between 2012 and 2019 as well as the decline in the rate of increase of HCFC-22.

This work is a promising step towards a more global monitoring of the halogenated substances, as the retrieval methodology can easily be applied to the whole IASI dataset. Future research will include the investigation of variability in the trends at regional/continental scale, with a particular interest in regions suspected of fugitive emissions or regions lacking in situ measurements (e.g., India, South America, Africa). Finally, there are other hyperspectral infrared nadir sounders in operation, such as AIRS on the NASA Aqua satellite [55] or CrIS (Cross-track Infrared Sounder) on Suomi-NPP satellite [56]. Both sounders provide radiance measurements with radiometric accuracy and stability [57,58] comparable to IASI and only a slightly coarser spectral resolution. They span the most useful spectral ranges but lack the region 1150–1210 cm^{-1} where HFC-134a and HCFC-142b have their prominent absorption bands. Therefore, a similar generalized least squares estimation approach could be applied to CrIS and AIRS measurements to retrieve the time evolution of CFC-11, CFC-12, HCFC-22, CF_4, SF_6 and CCl_4. The perspective to apply the methodology to the future hyperspectral infrared sounders (in particular IASI-NG [24]) will allow monitoring long-lived halogenated gases without interruptions for over 40 years.

Table 3
Annual mean vmrs, annual trends and normalized root-mean-square error (NRMSE).

Substance	Mean vmr (ppt)		Annual trend (ppt/year)			NRMSE	In situ network,
	2008	2021	2008–2021	2008–2011	2012–2021		spatial instrument
CFC-11	245	219	−1.6 ± 0.4	−3 ± 1	−1.5 ± 0.6[a]	0.01	IASI
	245	222	−1.6 ± 0.1	−2.1 ± 0.2	−1.6 ± 0.2	0.004	AGAGE
	246	226	−1.5 ± 0.2	−2.0 ± 0.6	−1.3 ± 0.3	0.007	ACE-FTS
CFC-12	539	487	−4.0 ± 0.8	−3 ± 2	−4 ± 1	0.01	IASI
	539	497	−3.2 ± 0.2	−2.6 ± 0.2	−3.5 ± 0.2	0.002	AGAGE
	537	502	−2.8 ± 0.3	−2.0 ± 0.7	−3.0 ± 0.4	0.003	ACE-FTS
HCFC-22	205	262	4.5 ± 0.7	7 ± 1	3.5 ± 0.8	0.02	IASI
	205	259	4.2 ± 0.6	7.0 ± 0.6	3.2 ± 0.5	0.02	AGAGE
	193	254	4.5 ± 0.6	8.0 ± 0.9	3.5 ± 0.4	0.02	ACE-FTS
HCFC-142b	21	27	0.3 ± 0.2	1.6 ± 0.4	0.2 ± 0.2	0.06	IASI
	21	23	0.1 ± 0.1	0.7 ± 0.1	−0.04 ± 0.05	0.03	AGAGE
	12	16	0.28 ± 0.09	0.8 ± 0.2	0.15 ± 0.08	0.04	ACE-FTS
HFC-134a	54	130	6.0 ± 0.3	5.2 ± 0.6	6.3 ± 0.5	0.03	IASI
	54	126	5.6 ± 0.2	5.0 ± 0.3	5.9 ± 0.2	0.01	AGAGE
	42	112	5.4 ± 0.3	5 ± 2	5.5 ± 0.3	0.03	ACE-FTS
CF_4	78	88	0.78 ± 0.06	0.62 ± 0.08	0.84 ± 0.08	0.005	IASI
	78	88	0.80 ± 0.03	0.62 ± 0.05	0.86 ± 0.03	0.003	AGAGE
	78	88	0.75 ± 0.06	0.6 ± 0.1	0.84 ± 0.05	0.005	ACE-FTS
SF_6	7	11	0.34 ± 0.03	0.29 ± 0.07	0.35 ± 0.04	0.02	IASI
	7	11	0.325 ± 0.007	0.28 ± 0.01	0.336 ± 0.006	0.006	AGAGE
	6	10	0.31 ± 0.02	0.3 ± 0.1	0.33 ± 0.03	0.02	ACE-FTS
CCl_4	89	72	−1.3 ± 0.3	−1 ± 1	−1.4 ± 0.5	0.03	IASI
	89	76	−1.03 ± 0.04	−1.1 ± 0.1	−1.00 ± 0.05	0.003	AGAGE
	90	76	−1.0 ± 0.3	−2 ± 1	−0.6 ± 0.4	0.03	ACE-FTS

[a]Two other CFC-11 trends were calculated with IASI: for the periods 2012–2018 (−1.3 ± 0.6 ppt/year) and 2019–2022 (−4 ± 1 ppt/year), see discussion for more details.

Table 4
Impact of profiles on annual trends 2008–2021.

Substance	Annual trend (ppt/year)		
	IASI		AGAGE
	ACE-FTS	*WACCM6*	
CFC-11	−1.6 ± 0.4	−1.5 ± 0.4	−1.6 ± 0.1
CFC-12	−4.0 ± 0.8	−3.7 ± 0.8	−3.2 ± 0.2
HCFC-22	4.5 ± 0.7	4.3 ± 0.7	4.2 ± 0.6
HCFC-142b	0.3 ± 0.2	0.3 ± 0.2	0.1 ± 0.1
CCl_4	−1.3 ± 0.3	−1.2 ± 0.3	−1.03 ± 0.04

Declaration of competing interest

The authors declare that they have no known competing financial interests or personal relationships that could have appeared to influence the work reported in this paper.

Data availability

Data will be made available on request.

Acknowledgments

IASI is a joint mission of EUMETSAT and the Centre National d'Études Spatiales (CNES, France). It is flown aboard the Metop satellites as part of the EUMETSAT Polar System. The IASI L1c data are received through the EUMETCast near-real-time data distribution service. H. De Longueville is grateful for her PhD grant to the "Fonds pour la Formation à la Recherche dans l'Industrie et dans l'Agriculture" of Belgium. L. Clarisse is a research associate supported by the Belgian F.R.S-FNRS. S. Whitburn is supported by the FED-tWIN ROLSS project funded via the Belgian Science Policy Office (BELSPO). The research in Belgium was funded by ESA-Belspo (HIRS project). The authors thank AERIS and EUMETSAT for providing us the reprocessed L1 IASI record. This project has received funding from the European Research Council (ERC) under the European Union's Horizon 2020 and innovation programme (grant agreement No 742909, IASI-FT advanced ERC grant). ACE-FTS data products are available at https://databace.scisat.ca/level2/ after sign-up (last accessed 21 February 2023). AGAGE data is available at https://agage2.eas.gatech.edu/data_archive/agage/ in open access (last accessed 31 January 2023).

Appendix. Trend uncertainty

In this appendix, we describe the development of a new metric that we use to estimate an uncertainty interval on the trend. Commonly, a confidence interval is used to estimate the margin error on the slope [19,22,59]. However, this metric suggests that by extending the time series, trends tend to be more precise despite the random variability within the concentrations. This does not reflect accurately the behavior of our results, as illustrated in Fig. A.5. We have therefore developed another metric which accounts for this random variability, based on a prediction interval as described below.

As explained in Section 2, the annual trend is derived from the fit of the time series (i.e., evolution of the concentration Y as a function of time T) with a simple linear regression:

$$Y(T) = \beta_0 + \beta_1 T + \epsilon \tag{A.1}$$

with the intercept β_0, the slope β_1 (i.e., the annual trend (ppt/year)) and the error term ϵ. The parameters β_0 and β_1 are estimated with a least squares estimation; and ϵ can be estimated by a prediction interval within which the true value of Y is likely to lie, with a specified level of confidence. This interval accounts both for the reducible error (uncertainty from the model) and the irreducible error (randomness of individual point which is not explained by the model) [59]. The estimated concentration $\hat{Y}$ is thus expressed as follows:

$$\hat{Y}(T) = (\hat{\beta}_0 + \hat{\beta}_1 T) \pm t_{\alpha/2,n-2} S \sqrt{1 + \frac{1}{n} + \frac{(T-\bar{T})^2}{\sum_{i=1}^{n}(T_i - \bar{T})^2}} \tag{A.2}$$

where $\hat{\beta}_0$ and $\hat{\beta}_1$ are the estimated parameters, $t_{\alpha/2,n-2}$ is the critical value of the t-distribution for $1-\alpha$ level of confidence and with $n-2$ degree of freedom (n corresponds to the number of points in the dataset and 2 is the number of parameters), $\bar{T}$ is the mean of T (i.e., the average

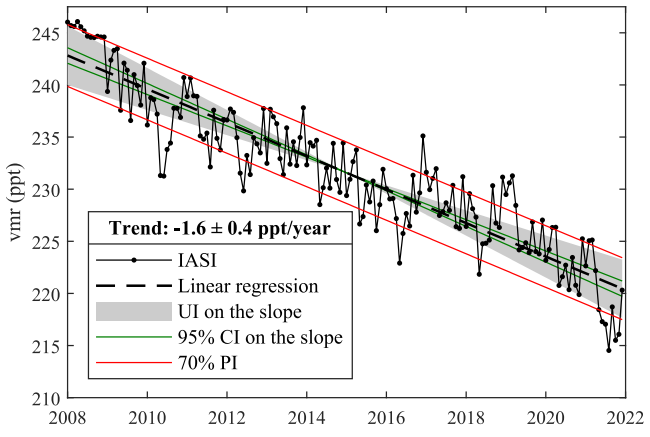

Fig. A.5. IASI time series of CFC-11 volume mixing ratio (similar to Fig. 3a) with the shaded uncertainty interval (UI) on the slope, the 95% confidence interval (CI) on the slope and the prediction interval (PI) for 70% level of confidence.

time) and $S = \sqrt{\frac{\sum_{i=1}^{n}(Y_i - \hat{Y}_i)^2}{n-2}}$ is the root-mean-square error (RMSE). Fig. A.5 illustrates the prediction interval associated to the IASI time series of CFC-11, for 70% level of confidence ($\alpha = 0.3$).

In this study n is large (e.g., $n = 168$ for IASI) and one can easily verify that the square root expression in Eq. (A.2) can be approximated to one. As $t_{\alpha/2,n-2}$ is also ≈ 1 for 70% level of confidence, the prediction interval is thus expressed by the RMSE.

From this prediction interval, we can express the trend with its uncertainty interval as:

$$\hat{\beta}_1 \pm \frac{S}{T_n - \bar{T}} \tag{A.3}$$

The slopes obtained in this way match the prediction interval from Eq. (A.2) at the extremes of the time series, as illustrated in Fig. A.5.

References

[1] World Meteorological Organization. Scientific Assessment of Ozone Depletion: 2022, GAW report no. 278. Geneva, Switzerland; 2022.

[2] World Meteorological Organization. Scientific Assessment of Ozone Depletion: 2018, Global Ozone Research and Monitoring Project–Report No. 58. Geneva, Switzerland; 2018.

[3] United Nations Environment Programme, Ozone Secretariat. Handbook for the montreal protocol on substances that deplete the ozone layer. 14th ed.. United Nations Environment Programme (UNEP); 2020.

[4] United Nations. Kyoto Protocol to the United Nations Framework Convention on Climate Change. 1997.

[5] Prinn RG, Weiss RF, Arduini J, Arnold T, DeWitt HL, Fraser PJ, Ganesan AL, Gasore J, Harth CM, Hermansen O, Kim J, Krummel PB, Li S, Loh ZM, Lunder CR, Maione M, Manning AJ, Miller BR, Mitrevski B, Mühle J, O'Doherty S, Park S, Reimann S, Rigby M, Saito T, Salameh PK, Schmidt R, Simmonds PG, Steele LP, Vollmer MK, Wang RH, Yao B, Yokouchi Y, Young D, Zhou L. History of chemically and radiatively important atmospheric gases from the advanced global atmospheric gases experiment (AGAGE). Earth Syst Sci Data 2018;10(2):985–1018. http://dx.doi.org/10.5194/essd-10-985-2018.

[6] Montzka SA, Dutton GS, Yu P, Ray E, Portmann RW, Daniel JS, Kuijpers L, Hall BD, Mondeel D, Siso C, Nance JD, Rigby M, Manning AJ, Hu L, Moore F, Miller BR, Elkins JW. An unexpected and persistent increase in global emissions of ozone-depleting CFC-11. Nature 2018;557(7705):413–7. http://dx.doi.org/10.1038/s41586-018-0106-2.

[7] Park S, Western LM, Saito T, Redington AL, Henne S, Fang X, Prinn RG, Manning AJ, Montzka SA, Fraser PJ, Ganesan AL, Harth CM, Kim J, Krummel PB, Liang Q, Mühle J, O'Doherty S, Park H, Park M-K, Reimann S, Salameh PK, Weiss RF, Rigby M. A decline in emissions of CFC-11 and related chemicals from eastern China. Nature 2021;590(7846):433–7. http://dx.doi.org/10.1038/s41586-021-03277-w.

[8] Western LM, Vollmer MK, Krummel PB, Adcock KE, Fraser PJ, Harth CM, Langenfelds RL, Montzka SA, Mühle J, O'Doherty S, Oram DE, Reimann S, Rigby M, Vimont I, Weiss RF, Young D, Laube JC. Global increase of ozone-depleting chlorofluorocarbons from 2010 to 2020. Nat Geosci 2023;16(4):309–13. http://dx.doi.org/10.1038/s41561-023-01147-w.

[9] Weiss RF, Ravishankara AR, Newman PA. Huge gaps in detection networks plague emissions monitoring. Nature 2021;595(7868):491–3. http://dx.doi.org/10.1038/d41586-021-01967-z.

[10] Prignon M, Chabrillat S, Minganti D, O'Doherty S, Servais C, Stiller G, Toon GC, Vollmer MK, Mahieu E. Improved FTIR retrieval strategy for HCFC-22 ($CHClF_2$), comparisons with in situ and satellite datasets with the support of models, and determination of its long-term trend above Jungfraujoch. Atmos Chem Phys 2019;19(19):12309–24. http://dx.doi.org/10.5194/acp-19-12309-2019.

[11] Zhou M, Vigouroux C, Langerock B, Wang P, Dutton G, Hermans C, Kumps N, Metzger J-M, Toon G, De Mazière M. CFC-11, CFC-12 and HCFC-22 ground-based remote sensing FTIR measurements at réunion island and comparisons with MIPAS/ENVISAT data. Atmos Meas Tech 2016;9(11):5621–36. http://dx.doi.org/10.5194/amt-9-5621-2016.

[12] Zhou M, Langerock B, Vigouroux C, Wang P, Hermans C, Stiller G, Walker KA, Dutton G, Mahieu E, De Mazière M. Ground-based FTIR retrievals of SF_6 on reunion island. Atmos Meas Tech 2018;11(2):651–62. http://dx.doi.org/10.5194/amt-11-651-2018.

[13] Pardo Cantos I, Mahieu E, Chipperfield MP, Smale D, Hannigan JW, Friedrich M, Fraser P, Krummel P, Prignon M, Makkor J, Servais C, Robinson J. Determination and analysis of time series of CFC-11 (CCl_3F) from FTIR solar spectra, in situ observations, and model data in the past 20 years above jungfraujoch (46°N), lauder (45°S), and cape grim (40°S) stations. Environ Sci: Atmos 2022;2(6):1487–501. http://dx.doi.org/10.1039/d2ea00060a.

[14] Coheur PF, Clerbaux C, Colin R. Spectroscopic measurements of halocarbons and hydrohalocarbons by satellite-borne remote sensors. J Geophys Res 2003;108(D4). http://dx.doi.org/10.1029/2002jd002649.

[15] Wetzel G, Höpfner M, Oelhaf H, Friedl-Vallon F, Kleinert A, Maucher G, Sinnhuber M, Abalichin J, Dehn A, Raspollini P. Long-term validation of MIPAS ESA operational products using MIPAS-B measurements. Atmos Meas Tech 2022;15(22):6669–704. http://dx.doi.org/10.5194/amt-15-6669-2022.

[16] Bernath PF, Steffen J, Crouse J, Boone CD. Sixteen-year trends in atmospheric trace gases from orbit. J Quant Spectrosc Radiat Transfer 2020;253:107–78. http://dx.doi.org/10.1016/j.jqsrt.2020.107178.

[17] Strow LL, DeSouza-Machado S. Establishment of AIRS climate-level radiometric stability using radiance anomaly retrievals of minor gases and SST. 2020, http://dx.doi.org/10.5194/amt-2019-504.

[18] Steffen J, Bernath PF, Boone CD. Trends in halogen-containing molecules measured by the atmospheric chemistry experiment (ACE) satellite. J Quant Spectrosc Radiat Transfer 2019;238:106619. http://dx.doi.org/10.1016/j.jqsrt.2019.106619.

[19] Chen A, Chen D, Hu X, Harth CM, Young D, Mühle J, Krummel PB, O'Doherty S, Weiss RF, Prinn RG, Fang X. Historical trend of ozone-depleting substances and hydrofluorocarbon concentrations during 2004–2020 derived from satellite observations and estimates for global emissions. Environ Pollut 2023;316:120570. http://dx.doi.org/10.1016/j.envpol.2022.120570.

[20] De Longueville H, Clarisse L, Whitburn S, Franco B, Bauduin S, Clerbaux C, Camy-Peyret C, Coheur P-F. Identification of short and long-lived atmospheric trace gases from IASI space observations. Geophys Res Lett 2021;48(5). http://dx.doi.org/10.1029/2020gl091742.

[21] Harries JE, Brindley HE, Sagoo PJ, Bantges RJ. Increases in greenhouse forcing inferred from the outgoing longwave radiation spectra of the earth in 1970 and 1997. Nature 2001;410(6826):355–7. http://dx.doi.org/10.1038/35066553.

[22] Chen X, Huang X, Strow LL. Near-global CFC-11 trends as observed by atmospheric infrared sounder from 2003 to 2018. J Geophys Res: Atmos 2020. http://dx.doi.org/10.1029/2020jd033051.

[23] Clerbaux C, Boynard A, Clarisse L, George M, Hadji-Lazaro J, Herbin H, Hurtmans D, Pommier M, Razavi A, Turquety S, Wespes C, Coheur P-F. Monitoring of atmospheric composition using the thermal infrared IASI/MetOp sounder. Atmos Chem Phys 2009;9(16):6041–54. http://dx.doi.org/10.5194/acp-9-6041-2009.

[24] Crevoisier C, Clerbaux C, Guidard V, Phulpin T, Armante R, Barret B, Camy-Peyret C, Chaboureau J-P, Coheur P-F, Crépeau L, Dufour G, Labonnote L, Lavanant L, Hadji-Lazaro J, Herbin H, Jacquinet-Husson N, Payan S, Péquignot E, Pierangelo C, Sellitto P, Stubenrauch C. Towards IASI-new generation (IASI-NG) : impact of improved spectral resolution and radiometric noise on the retrieval of thermodynamic, chemistry and climate variables. Atmos Meas Tech 2014;7(12):4367–85. http://dx.doi.org/10.5194/amt-7-4367-2014.

[25] George M, Clerbaux C, Bouarar I, Coheur P-F, Deeter MN, Edwards DP, Francis G, Gille JC, Hadji-Lazaro J, Hurtmans D, Inness A, Mao D, Worden HM. An examination of the long-term CO records from MOPITT and IASI: comparison of retrieval methodology. Atmos Meas Tech 2015;8(10):4313–28. http://dx.doi.org/10.5194/amt-8-4313-2015.

[26] Gaudel A, Cooper OR, Ancellet G, Barret B, Boynard A, Burrows JP, Clerbaux C, Coheur P-F, Cuesta J, Cuevas E, Doniki S, Dufour G, Ebojie F, Foret G, Garcia O, Granados-Muñoz MJ, Hannigan JW, Hase F, Hassler B, Huang G, Hurtmans D, Jaffe D, Jones N, Kalabokas P, Kerridge B, Kulawik S, Latter B, Leblanc T, Le Flochmoën E, Lin W, Liu J, Liu X, Mahieu E, McClure-Begley A, Neu JL, Osman M, Palm M, Petetin H, Petropavlovskikh I, Querel R, Rahpoe N, Rozanov A, Schultz MG, Schwab J, Siddans R, Smale D, Steinbacher M, Tanimoto H, Tarasick DW, Thouret V, Thompson AM, Trickl T, Weatherhead E, Wespes C, Worden HM, Vigouroux C, Xu X, Zeng G, Ziemke J. Tropospheric

ozone assessment report: Present-day distribution and trends of tropospheric ozone relevant to climate and global atmospheric chemistry model evaluation. Elementa: Sci Anthropoc 2018;6. http://dx.doi.org/10.1525/elementa.291.

[27] Van Damme M, Clarisse L, Franco B, Sutton MA, Erisman JW, Kruit RW, van Zanten M, Whitburn S, Hadji-Lazaro J, Hurtmans D, Clerbaux C, Coheur P-F. Global, regional and national trends of atmospheric ammonia derived from a decadal (2008–2018) satellite record. Environ Res Lett 2021;16(5):055017. http://dx.doi.org/10.1088/1748-9326/abd5e0.

[28] Wespes C, Hurtmans D, Clerbaux C, Boynard A, Coheur P-F. Decrease in tropospheric O_3 levels in the northern hemisphere observed by IASI. Atmos Chem Phys 2018;18(9):6867–85. http://dx.doi.org/10.5194/acp-18-6867-2018.

[29] Wespes C, Hurtmans D, Chabrillat S, Ronsmans G, Clerbaux C, Coheur P-F. Is the recovery of stratospheric O_3 speeding up in the southern hemisphere? An evaluation from the first IASI decadal record (2008–2017). Atmos Chem Phys 2019;19(22):14031–56. http://dx.doi.org/10.5194/acp-19-14031-2019.

[30] Wespes C, Ronsmans G, Clarisse L, Solomon S, Hurtmans D, Clerbaux C, Coheur P-F. Polar stratospheric nitric acid depletion surveyed from a decadal dataset of IASI total columns. Atmos Chem Phys 2022;22(16):10993–1007. http://dx.doi.org/10.5194/acp-22-10993-2022.

[31] Whitburn S, Clarisse L, Bouillon M, Safieddine S, George M, Dewitte S, De Longueville H, Coheur P-F, Clerbaux C. Trends in spectrally resolved outgoing longwave radiation from 10 years of satellite measurements. NPJ Clim Atmos Sci 2021;4(1). http://dx.doi.org/10.1038/s41612-021-00205-7.

[32] Kessy A, Lewin A, Strimmer K. Optimal whitening and decorrelation. Amer Statist 2018;72(4):309–14. http://dx.doi.org/10.1080/00031305.2016.1277159.

[33] von Clarmann T, Grabowski U, Kiefer M. On the role of non-random errors in inverse problems in radiative transfer and other applications. J Quant Spectrosc Radiat Transfer 2001;71(1):39–46. http://dx.doi.org/10.1016/s0022-4073(01)00010-3.

[34] Walker JC, Carboni E, Dudhia A, Grainger RG. Improved detection of sulphur dioxide in volcanic plumes using satellite-based hyperspectral infrared measurements: Application to the eyjafjallajökull 2010 eruption. J Geophys Res: Atmos 2012;117(D20). http://dx.doi.org/10.1029/2011jd016810.

[35] Rodgers CD. Inverse methods for atmospheric sounding. World Scientific; 2000, http://dx.doi.org/10.1142/3171.

[36] Walker JC, Dudhia A, Carboni E. An effective method for the detection of trace species demonstrated using the metop infrared atmospheric sounding interferometer. Atmos Meas Tech 2011;4(8):1567–80. http://dx.doi.org/10.5194/amt-4-1567-2011.

[37] Theys N, Fioletov V, Li C, De Smedt I, Lerot C, McLinden C, Krotkov N, Griffin D, Clarisse L, Hedelt P, Loyola D, Wagner T, Kumar V, Innes A, Ribas R, Hendrick F, Vlietinck J, Brenot H, Van Roozendael M. A sulfur dioxide covariance-based retrieval algorithm (COBRA): application to TROPOMI reveals new emission sources. Atmos Chem Phys 2021;21(22):16727–44. http://dx.doi.org/10.5194/acp-21-16727-2021.

[38] Whitburn S, Clarisse L, Crapeau M, August T, Hultberg T, Coheur PF, Clerbaux C. A CO_2-independent cloud mask from infrared atmospheric sounding interferometer (IASI) radiances for climate applications. Atmos Meas Tech 2022;15(22):6653–68. http://dx.doi.org/10.5194/amt-15-6653-2022.

[39] Bouillon M, Safieddine S, Hadji-Lazaro J, Whitburn S, Clarisse L, Doutriaux-Boucher M, Coppens D, August T, Jacquette E, Clerbaux C. Ten-year assessment of IASI radiance and temperature. Remote Sens 2020;12(15):2393. http://dx.doi.org/10.3390/rs12152393.

[40] Coheur P-F, Barret B, Turquety S, Hurtmans D, Hadji-Lazaro J, Clerbaux C. Retrieval and characterization of ozone vertical profiles from a thermal infrared nadir sounder. J Geophys Res 2005;110(D24). http://dx.doi.org/10.1029/2005jd005845.

[41] Rothman LS, Gordon IE, Babikov Y, Barbe A, Benner DC, Bernath PF, Birk M, Bizzocchi L, Boudon V, Brown LR, Campargue A, Chance K, Cohen EA, Coudert LH, Devi VM, Drouin BJ, Fayt A, Flaud J-M, Gamache RR, Harrison JJ, Hartmann J-M, Hill C, Hodges JT, Jacquemart D, Jolly A, Lamouroux J, Roy RJL, Li G, Long DA, Lyulin OM, Mackie CJ, Massie ST, Mikhailenko S, Müller HSP, Naumenko OV, Nikitin AV, Orphal J, Perevalov V, Perrin A, Polovtseva ER, Richard C, Smith MAH, Starikova E, Sung K, Tashkun S, Tennyson J, Toon GC, Tyuterev VG, Wagner G. The HITRAN2012 molecular spectroscopic database. J Quant Spectrosc Radiat Transfer 2013;130:4–50. http://dx.doi.org/10.1016/j.jqsrt.2013.07.002.

[42] Copernicus Climate Change Service. ERA5 monthly averaged data on pressure levels from 1979 to present. 2019, http://dx.doi.org/10.24381/CDS.6860A573.

[43] Copernicus Climate Change Service. ERA5 monthly averaged data on single levels from 1979 to present. 2019, http://dx.doi.org/10.24381/CDS.F17050D7.

[44] Hersbach H, Bell B, Berrisford P, Hirahara S, Horányi A, Muñoz-Sabater J, Nicolas J, Peubey C, Radu R, Schepers D, Simmons A, Soci C, Abdalla S, Abellan X, Balsamo G, Bechtold P, Biavati G, Bidlot J, Bonavita M, Chiara G, Dahlgren P, Dee D, Diamantakis M, Dragani R, Flemming J, Forbes R, Fuentes M, Geer A, Haimberger L, Healy S, Hogan RJ, Hólm E, Janisková M, Keeley S, Laloyaux P, Lopez P, Lupu C, Radnoti G, Rosnay P, Rozum I, Vamborg F, Villaume S, Thépaut J-N. The ERA5 global reanalysis. Q J R Meteorol Soc 2020;146(730):1999–2049. http://dx.doi.org/10.1002/qj.3803.

[45] Kneizys FX, Abreu LW, Anderson GP, Chetwynd JH, Shettle EP, Berk A, Bernstein LS, Robertson DC, Acharya P, Rothman LS, Selby JEA, Gallery WO, Clough SA. The MODTRAN2/3 report and LOWTRAN 7 model. Phillips Laboratory, Geophysics Directorat; 1996.

[46] Bernath PF, Crouse J, Hughes RC, Boone CD. The atmospheric chemistry experiment Fourier transform spectrometer (ACE-FTS) version 4.1 retrievals: Trends and seasonal distributions. J Quant Spectrosc Radiat Transfer 2021;259:107409. http://dx.doi.org/10.1016/j.jqsrt.2020.107409.

[47] Montzka SA, Dutton GS, Portmann RW, Chipperfield MP, Davis S, Feng W, Manning AJ, Ray E, Rigby M, Hall BD, Siso C, Nance JD, Krummel PB, Mühle J, Young D, O'Doherty S, Salameh PK, Harth CM, Prinn RG, Weiss RF, Elkins JW, Walter-Terrinoni H, Theodoridi C. A decline in global CFC-11 emissions during 2018–2019. Nature 2021;590(7846):428–32. http://dx.doi.org/10.1038/s41586-021-03260-5.

[48] Rigby M, Park S, Saito T, Western LM, Redington AL, Fang X, Henne S, Manning AJ, Prinn RG, Dutton GS, Fraser PJ, Ganesan AL, Hall BD, Harth CM, Kim J, Kim K-R, Krummel PB, Lee T, Li S, Liang Q, Lunt MF, Montzka SA, Mühle J, O'Doherty S, Park M-K, Reimann S, Salameh PK, Simmonds P, Tunnicliffe RL, Weiss RF, Yokouchi Y, Young D. Increase in CFC-11 emissions from eastern China based on atmospheric observations. Nature 2019;569(7757):546–50. http://dx.doi.org/10.1038/s41586-019-1193-4.

[49] Kim J, Thompson R, Park H, Bogle S, Mühle J, Park M-K, Kim Y, Harth CM, Salameh PK, Schmidt R, Ottinger D, Park S, Weiss RF. Emissions of tetrafluoromethane (CF_4) and hexafluoroethane (C_2F_6) from east Asia: 2008 to 2019. J Geophys Res: Atmos 2021;126(16). http://dx.doi.org/10.1029/2021jd034888.

[50] Simmonds PG, Rigby M, Manning AJ, Park S, Stanley KM, McCulloch A, Henne S, Graziosi F, Maione M, Arduini J, Reimann S, Vollmer MK, Mühle J, O'Doherty S, Young D, Krummel PB, Fraser PJ, Weiss RF, Salameh PK, Harth CM, Park M-K, Park H, Arnold T, Rennick C, Steele LP, Mitrevski B, Wang RHJ, Prinn RG. The increasing atmospheric burden of the greenhouse gas sulfur hexafluoride (SF_6). Atmos Chem Phys 2020;20(12):7271–90. http://dx.doi.org/10.5194/acp-20-7271-2020.

[51] Kovács T, Feng W, Totterdill A, Plane JMC, Dhomse S, Gómez-Martín JC, Stiller GP, Haenel FJ, Smith C, Forster PM, García RR, Marsh DR, Chipperfield MP. Determination of the atmospheric lifetime and global warming potential of sulfur hexafluoride using a three-dimensional model. Atmos Chem Phys 2017;17(2):883–98. http://dx.doi.org/10.5194/acp-17-883-2017.

[52] Gettelman A, Mills MJ, Kinnison DE, Garcia RR, Smith AK, Marsh DR, Tilmes S, Vitt F, Bardeen CG, McInerny J, Liu H-L, Solomon SC, Polvani LM, Emmons LK, Lamarque J-F, Richter JH, Glanville AS, Bacmeister JT, Phillips AS, Neale RB, Simpson IR, DuVivier AK, Hodzic A, Randel WJ. The whole atmosphere community climate model version 6 (WACCM6). J Geophys Res: Atmos 2019;124(23):12380–403. http://dx.doi.org/10.1029/2019jd030943.

[53] Hannigan JW, Ortega I, Shams SB, Blumenstock T, Campbell JE, Conway S, Flood V, Garcia O, Griffith D, Grutter M, Hase F, Jeseck P, Jones N, Mahieu E, Makarova M, De Mazière M, Morino I, Murata I, Nagahama T, Nakijima H, Notholt J, Palm M, Poberovskii A, Rettinger M, Robinson J, Röhling AN, Schneider M, Servais C, Smale D, Stremme W, Strong K, Sussmann R, Te Y, Vigouroux C, Wizenberg T. Global atmospheric OCS trend analysis from 22 NDACC stations. J Geophys Res: Atmos 2022;127(4). http://dx.doi.org/10.1029/2021jd035764.

[54] De Mazière M, Thompson AM, Kurylo MJ, Wild JD, Bernhard G, Blumenstock T, Braathen GO, Hannigan JW, Lambert J-C, Leblanc T, McGee TJ, Nedoluha G, Petropavlovskikh I, Seckmeyer G, Simon PC, Steinbrecht W, Strahan SE. The network for the detection of atmospheric composition change (NDACC): history, status and perspectives. Atmos Chem Phys 2018;18(7):4935–64. http://dx.doi.org/10.5194/acp-18-4935-2018.

[55] Aumann HH, Chahine MT, Gautier C, Goldberg MD, Kalnay E, McMillin LM, Revercomb H, Rosenkranz PW, Smith WL, Staelin DH, Strow LL, Susskind J. AIRS/AMSU/HSB on the aqua mission: design, science objectives, data products, and processing systems. IEEE Trans Geosci Remote Sens 2003;41(2):253–64. http://dx.doi.org/10.1109/tgrs.2002.808356.

[56] Han Y, Revercomb H, Cromp M, Gu D, Johnson D, Mooney D, Scott D, Strow L, Bingham G, Borg L, Chen Y, DeSlover D, Esplin M, Hagan D, Jin X, Knuteson R, Motteler H, Predina J, Suwinski L, Taylor J, Tobin D, Tremblay D, Wang C, Wang L, Wang L, Zavyalov V. Suomi NPP CrIS measurements, sensor data record algorithm, calibration and validation activities, and record data quality. J Geophys Res: Atmos 2013;118(22):12,734–48. http://dx.doi.org/10.1002/2013jd020344.

[57] Aumann HH, Broberg S, Manning E, Pagano T. Radiometric stability validation of 17 years of AIRS data using sea surface temperatures. Geophys Res Lett 2019;46(21):12504–10. http://dx.doi.org/10.1029/2019gl085098.

[58] Strow LL, Motteler H, Tobin D, Revercomb H, Hannon S, Buijs H, Predina J, Suwinski L, Glumb R. Spectral calibration and validation of the cross-track infrared sounder on the suomi NPP satellite. J Geophys Res: Atmos 2013;118(22):12,486–96. http://dx.doi.org/10.1002/2013jd020480.

[59] Devore JL, Berk KN. Modern mathematical statistics with applications. Springer New York; 2012, http://dx.doi.org/10.1007/978-1-4614-0391-3.